14th International Symposium on Turbulence and Shear Flow Phenomena (TSFP14)
Heidelberg, Germany, July 28–31, 2026

BUBBLE INTERACTION DYNAMICS AND ACOUSTIC SIGNATURE DUE TO COALESCENCE, IMPINGEMENT, AND FRAGMENTATION

Suraj Narayan Dhar
Department of Applied Mechanics
IIT Delhi
New Delhi
amz228092@iitd.ac.in

Narsing K. Jha
Department of Applied Mechanics
IIT Delhi
New Delhi
narsingjha@am.iitd.ac.in

ABSTRACT
The acoustic emissions associated with evolving bubble dynamics were investigated experimentally for three bubble-chain release rates, $f_b = 20$, 32, and 47 Hz. Bubbles generated underwater from a submerged nozzle exhibited a range of complex interaction events, including necking and detachment of the primary bubble, primary and secondary coalescence, impingement, and subsequent fragmentation into smaller bubbles farther downstream. The acoustic responses corresponding to these events were analyzed through synchronization of high-speed imaging with temporal acoustic measurements. The bubble interactions with increase in f_b near the nozzle and breakup in the downstream led to a progressive reduction in the dominant resonant frequency bands , which decreased from 860 Hz to 659 Hz and 439 Hz for $f_b = 20$, 32, and 47 Hz, respectively. The sound pressure level (SPL) increased with f_b within the respective dominant frequency bands. The impingement and coalescence phenomena enhanced the peak acoustic pressure but their contributions remained less significant than those associated with necking and bubble pinch-off. At farther downstream, the fragmentation of the bubble cluster gave rise to a collective low-frequency acoustic mode, which became localized within a relatively narrow frequency region.

INTRODUCTION
Bubble acoustics has been extensively studied since the early 1900s, owing to its importance in diverse applications ranging from drug delivery in biomedical systems , stealth technologies in the defense industry and many more. Pioneering contributions were made by Rayleigh (1917), Leighton (2012), and Strasberg (1956). Bubbles are commonly modeled as spring-like systems due to the compressibility of the enclosed gas, exhibiting oscillator-like behavior that generates pressure fluctuations in the surrounding liquid. Minnaert (1933) derived the natural oscillation frequency of a single, spherically pulsating bubble as

$$f = \frac{1}{2\pi R_0}\sqrt{\frac{3\gamma p_0}{\rho}}, \qquad (1)$$

where R is the bubble radius, γ is the ratio of specific heats of the gas, p_0 is the ambient pressure, and ρ is the liquid density. In the case of bubble chains, however, the resonant frequency often deviates from Minnaert's prediction due to mutual coupling and interference among neighboring oscillating bubbles.At higher bubbling rates, secondary bubbles detach more rapidly than primary bubbles, leading to interactions such as coalescence, rebound, or penetration. These clustered dynamics often result in fragmentation into multiple daughter bubbles downstream. The resulting acoustic radiation exhibits complex interference patterns, as in-phase and out-of-phase oscillations within the chain modulate the overall sound signature (Hsiao *et al.* (2001),Manasseh *et al.* (2004)).

In this study, experiments were conducted at three bubbling rates of 20, 32, and 47 Hz. The morphological evolution of the bubble chain, including multiple bubble interaction events at different f_b, was investigated using high-speed shadowgraph imaging together with the corresponding acoustic response acquired at two different regimes. Particular attention was given to the acoustic characteristics and the shift in resonant frequency as the flow evolved from a chain of single bubbles with finite inter-bubble spacing to a bubble plume consisting of strongly interacting bubbles downstream of detachment with increasing bubbling rate, f_b.

EXPERIMENTAL SETUP AND METHODOLOGY
The experiments were conducted in a glass tank of dimensions $1.5\,\mathrm{m} \times 1\,\mathrm{m} \times 1\,\mathrm{m}$, as shown in Fig. 1. Bubbles were generated at the bottom of the tank through a submerged circular nozzle of inner diameter 2 mm, while the bubbling rate, f_b, was regulated using a syringe pump. Driven by buoyancy, the bubbles rose through the liquid and underwent various interaction phenomena downstream, including coalescence, impingement, and fragmentation. These dynamics were captured using the shadowgraph technique, a non-invasive optical method in which the camera records the shadow of the region of interest. Illumination was provided from the opposite side of the tank, and a diffuser sheet was used to ensure a homogeneous distribution of light across the field of view. A pair of high-speed cameras (Photron Mini UX-100) were employed in two adjacent planes, namely the x–y and y–z planes, operating at 2000 fps with a shutter speed of $1/4000$, to capture the morphological evolution of bubbles both near the nozzle and farther downstream. Acoustic signals were recorded using two hydrophones: one positioned near the nozzle and the other placed approximately 25 cm axially downstream of the nozzle. These measurements were intended to capture detachment, impingement, and coalescence events near the nozzle, as well as fragmentation events farther downstream.

The acoustic signals were acquired at two locations: first, in the near-nozzle region, approximately 10 cm axially away from the nozzle; and second, at a downstream location 20 cm along the bubble chain and 10 cm axially away from it. The signals were recorded at a sampling rate of 100 kS/s. Since the bubble-generated acoustic signals were of low amplitude, the hydrophone outputs were amplified using a preamplifier with a gain of 40 dB for all cases. The preamplifier was equipped with high-pass and low-pass filters in the range of 200–5000 Hz to resolve the dominant and resonant frequency components. The processed signals were acquired using a DAQ (PicoScope) to ensure simultaneous measurement of the high-speed images and the acoustic response. Both the hydrophones and the high-speed cameras were synchronized through TTL links, enabling precise correlation of individual bubble events with their corresponding acoustic signatures. The acquired voltage signal was converted into an acoustic pressure signal using Eq. 2:

$$\mathrm{SPL} = 20\log_{10}\left(\frac{p}{p_{\mathrm{ref}}}\right) = 20\log_{10}(V) + 211 - \mathrm{Gain} \qquad (2)$$

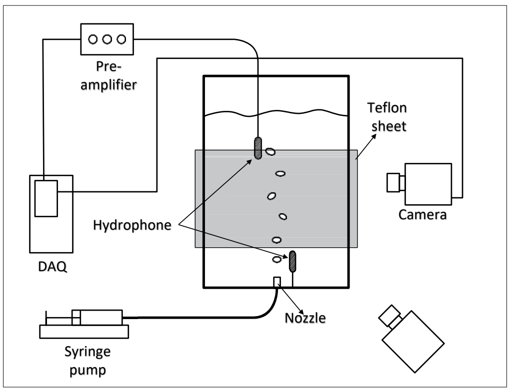

Figure 1. 2-D schematic of the experimental setup showing high-speed imaging and acoustic measurements in the near-nozzle region and at a far-field location downstream of the nozzle.

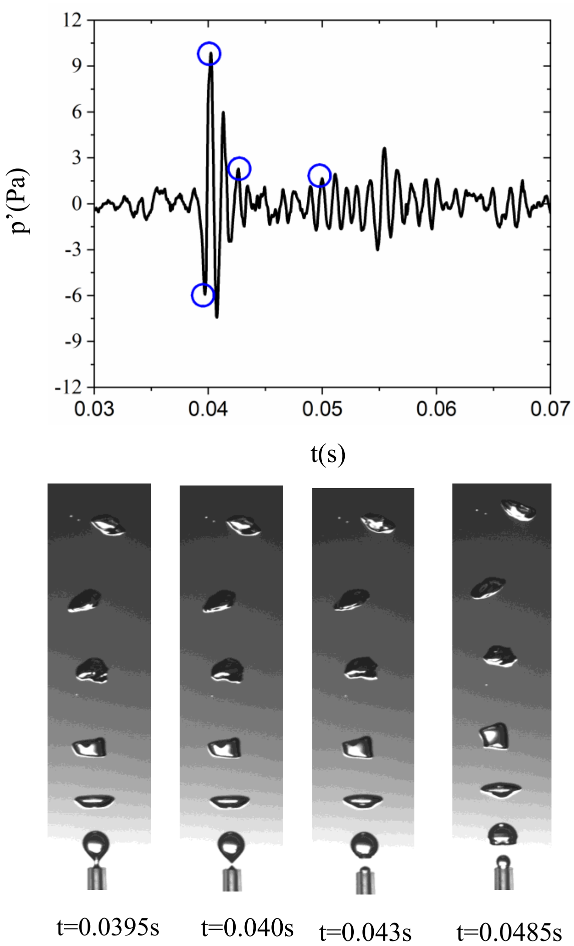

Figure 2. Acoustic response of the bubble chain at a bubbling rate of $f_b = 20$ Hz acquired near the nozzle. The circled time instants indicate the corresponding events identified in the synchronized shadowgraph images.

RESULTS AND DISCUSSION

0.1 Bubble dynamics and acoustic response at $f_b = 20$ Hz

The equivalent bubble diameter, d_{eq}, was measured immediately after detachment using the major axis, d_{maj}, and minor axis, d_{min}, obtained from both the x–z and y–z planes, according to $d_{eq} = \sqrt[3]{d_{\mathrm{maj}}^2 d_{\mathrm{min}}}$, as listed in Table 1. The resonant frequency, denoted by f_m, decreases with increasing bubbling rate, f_b, because larger bubbles accelerate a greater mass of the surrounding liquid, thereby slowing the volumetric oscillation and increasing the acoustic wavelength. The synchronized high-speed images and the corresponding acoustic measurements acquired near the nozzle for $f_b = 20$ Hz, shown in Fig. 2, indicate that the individual bubbles in the chain maintain an inter-bubble spacing of approximately 1 cm. The primary events observed in this case are the acoustic emission during bubble necking prior to pinch-off, followed by pinch-off itself, and subsequently the shape oscillations of multiple bubbles. A distinct dip in the acoustic signature is observed at $t = 0.0395$ s, corresponding to the necking of the bubble. This dip arises because the rapid inward acceleration of air during necking produces a suction effect in the surrounding liquid, drawing the fluid inward and causing a negative excursion in the acoustic pressure.Immediately afterward, a sharp rise in acoustic pressure is observed at $t = 0.04$ s. This increase corresponds to the volumetric pulsation of the bubble just after detachment from the nozzle. Following detachment, the acoustic pulse gradually decreases in magnitude and subsequently exhibits an uneven amplitude before decaying completely. At $t = 0.043$ and $t = 0.0485$ s, the recorded pressure is predominantly influenced by the presence of multiple bubbles in the chain and represents the superposition of the acoustic pressure radiated by the neighboring bubbles. The contribution of shape oscillation to the radiated acoustic pressure remains relatively weak (Strasberg (1956); Longuet-Higgins (1989)). The energy transferred to the neighboring bubbles during the detachment of the newly formed bubble excites their oscillations. Owing to the small inter-bubble spacing, these multiple-bubble oscillations give rise to strong coupling effects (Feuillade (2001),Tolstoy (1986)), which reduce the resonant frequency f_m, as reflected by the observed peak frequency f_0 listed in Table 1.

Table 1. Bubble chain characteristics showing the equivalent bubble diameter, resonant frequency (f_m), observed peak frequency (f_0), and acoustic wavelength (λ) at different bubbling rates.

f_b (Hz)	d_{eq} (mm)	f_m (Hz)	f_0 (Hz)	λ (mm)
20	5.6	1164	860	1290
32	6.4	1018	659	1473
47	7.2	905	439	1657

0.2 Bubble dynamics and acoustic response at $f_b = 32$ Hz

The same initial dip and subsequent rise in the acoustic signal are observed at $f_b = 32$ Hz in Fig. 3(a), corresponding to the necking and volumetric pulsation stages at $t = 0.028$ s and 0.029 s, respectively. The acoustic pressure associated with volumetric pulsation increases by approximately 1.5 times and the dip in acoustic pressure due to necking increases by about 1.2 times, as f_b increases from 20 Hz to 32 Hz. At this higher bubbling rate, the increased buoyancy force and the transfer of energy from the newly detached bubble to the neighboring bubble undergo bubble coalescence, which is observed to occur approximately 3 cm downstream of the nozzle. The coalesced bubbles continue to rise under buoyancy, and the corresponding acoustic response measured 20 cm downstream is shown in Fig. 3(b). A rise in acoustic pressure is observed due to coalescence and subsequent fragmentation at the downstream location, as evident at $t = 0.13$ s. At later time instants, $t = 0.134$ s and $t = 0.137$ s, the acoustic pressure exhibits alternating rise and fall, which may be attributed to the in-phase and out-of-phase oscillations of the multiple fragmented bubbles present within the measurement zone. In the case of a bubble chain, the individual acoustic contributions arising from fragmentation and coalescence are difficult to distinguish in the pressure signal, as the measured response represents the superposition of sound radiated by multiple bubbles undergoing different complex events at their respective locations. It is observed that fragmentation and coalescence produce acoustic pressure amplitudes comparable to those associated with necking; however, they remain lower than the sound generated during volumetric pulsation, with peak values reaching nearly half of the pressure amplitude radiated at detachment.

0.3 Bubble dynamics and acoustic response at $f_b = 47$ Hz

At this higher bubbling rate, several complex interaction events are observed near the nozzle at different time instants, namely $t = 0.0138$, 0.0144, 0.043, 0.0435, 0.0676, and 0.0682 s, as shown in Fig. 4. The time instants $t = 0.0138$, 0.043, and 0.0676 s corresponds to the sound radiated due to necking however, the associated pressure amplitude varies at these instants due to the presence of three different morphological evolution of bubble.The negative pressure amplitude changes from -11.6 Pa at $t = 0.0138$ s to -7 Pa at $t = 0.043$ s, which may be attributed to the impingement of the newly forming bubble on the recently detached one. The impingement event radiates a positive acoustic pressure however, its amplitude remains lower than that of the necking sound. Further, at $t = 0.0676$ s, the pressure amplitude reaches -12.7 Pa, which may be attributed to the simultaneous occurrence of coalescence between the primary and secondary bubbles and the necking of the newly generated bubble. The coalescence and impingement phenomena are found to increase the acoustic pressure however, they are comparatively weaker sources of sound generation because they do not involve significant net volumetric displacement. Instead, these events are primarily associated with shape oscillations, which radiate sound less efficiently and therefore contribute more weakly to the overall acoustic field.

Further, a sharp rise in acoustic pressure is observed in the near-field signal at three different time instants, namely $t = 0.0144$, 0.0435, and 0.0682 s, which correspond to the volumetric pulsation during bubble detachment. The volumetric pulsation during pinchoff and the additional coupled oscillation from bubbles in chain enhance the acoustic pressure. The acoustic pressure amplitude varies at these three instants due to the differences in bubble dynamics associated with each event. The single bubble pinch off and the coupled oscillation from neighbouring bubble at $t = 0.0144$ rises the peak to 17.09 Pa but due to the primary coalescence at 0.0435 during pinchoff reduces the acosutic peak to 15 Pa. This reduction in acoustic pressure is attributed to the supression offered by the coalesced neighbouring bubble on the pinch off phenomena. Further, at $t = 0.0682$ s, the combined acoustic emission from the newly detached bubble and the coalescence of neighboring bubbles with the detached bubble increases the measured acoustic pressure by nearly 1.5 times.

Away from the nozzle , the coalesced bubbles are observed to fragment into multiple bubbles of varying diameters, ranging from $d_{eq}/7$ to $1.5\,d_{eq}$. The corresponding peak acoustic pressure decreases by a factor of approximately 3 compared to the sound radiated during volumetric pulsation. The coupled oscillations of these multiple fragmented bubbles in the downstream region also influence the acoustic response and thereby affect the resonant frequency, as discussed in Fig. **??**. The superposition of sound radiated by multiple fragmented bubbles, together with the phase lag among them, leads to an increase or decrease in the acoustic response measured at a location 10 cm axially away from the bubble chain.

0.4 Effect on resonant frequencies and Sound pressure level near the nozzle

The near-nozzle regime is characterized by events such as volumetric pulsation, primary coalescence (between the newly forming bubble and its nearest neighboring bubble), secondary coalescence (between neighboring bubbles other than the newly forming bubble), impingement, and the influence of multiple coalesced bubbles farther downstream, all of which play a significant role in altering the resonant frequency. At $f_b = 20$ Hz, as shown in Fig. 5(a,b), a stable narrowband dominant component persists in the frequency range of approximately 0.78–0.92 kHz, representing a reduction of about 33% relative to f_m. The corresponding SPL confirms the presence of the same dominant frequency band, with values in the range of 92–95 dB. The weaker horizontal bands above and below the dominant component indicate additional acoustic responses associated with coupled oscillations in the nearby downstream region.

With increasing bubbling rate, the complex events occurring near the nozzle tend to suppress the influence of coupled oscillations farther downstream. Consequently, Fig. 5(c,d) for $f_b = 32$ Hz does not show the weaker horizontal bands ob-

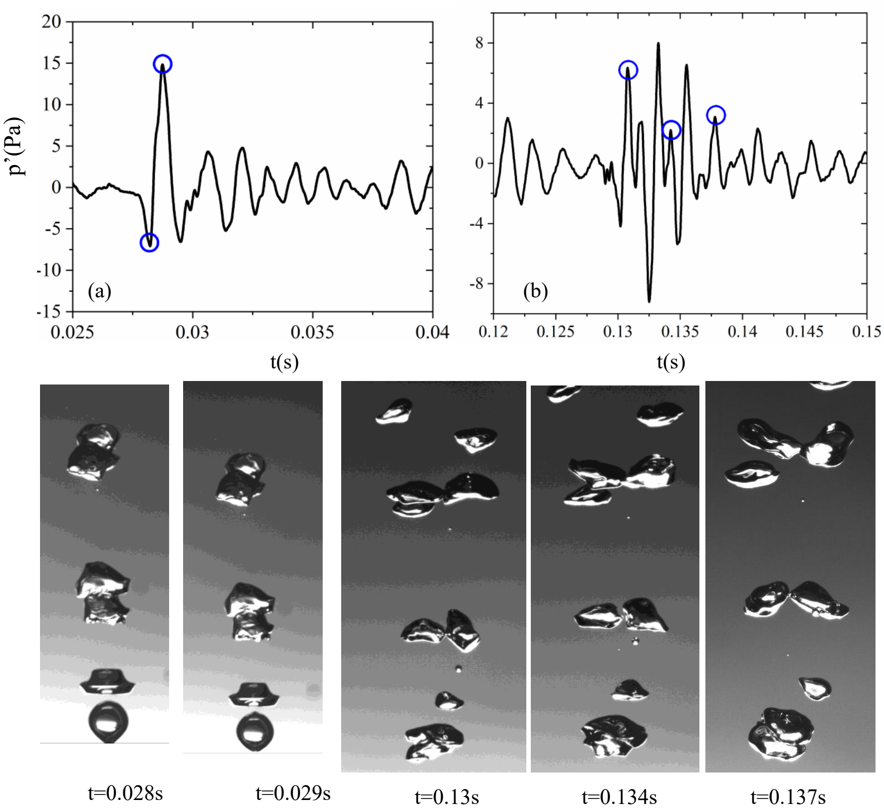

Figure 3. Acoustic response of the bubble chain at a bubbling rate of $f_b = 32$ Hz. (a) signals acquired near the nozzle and (b) signals acquired 20cm axially away from the nozzle. The circled time instants indicate the corresponding events identified in the synchronized shadowgraph images.

served at $f_b = 20$ Hz. Instead, a dominant narrowband component is observed in the range of approximately 520–700 Hz, while the SPL within this dominant band increases to about 97–105 dB.

A further increase in bubbling rate to $f_b = 47$ Hz leads to the appearance of a broader dominant narrowband region extending from approximately 400 to 850 Hz. This broadening may be attributed to the oscillation of multiple fragmented bubbles of different sizes, each exhibiting a distinct phase lag within the chain, together with the effects of primary coalescence near the nozzle and secondary coalescence farther downstream. The SPL further increases to 105–110 dB within the dominant frequency regime near the nozzle with increasing f_b, indicating enhanced acoustic pressure radiation.

0.5 Effect on resonant frequencies and Sound pressure level away from the nozzle

At $f_b = 20$ Hz in Fig.6(a), the dominant narrowband component broadens to approximately 700–980 Hz due to the presence of multiple bubbles in the chain with finite inter-bubble spacing, which activates coupled oscillations among them. The phase lag between bubbles gives rise to constructive and destructive interference, thereby modifying the dominant frequency band and the corresponding SPL to approximately 88–93 dB within this range. With a further increase in f_b to 32 Hz and 47 Hz in Fig.6(c,e) , fragmentation of the coalesced bubbles is observed. In both cases, the dominant frequency band becomes more localized and shifts to lower frequencies, occurring near 500 Hz for $f_b = 32$ Hz and 410 Hz for $f_b = 47$ Hz. As the number of fragmented bubbles increases with f_b, the bubbles remain closely spaced and collectively oscillate as a larger equivalent bubble cluster, giving rise to a lower dominant frequency. Thus, the reduced spectral broadening observed at higher f_b is more appropriately attributed to the emergence of a dominant collective low-frequency mode than to a suppression of coupling by fragmentation.

The SPL spectrograms in Fig.5(b,d,f) show that, with increasing bubbling rate f_b, the dominant acoustic band progressively shifts toward lower frequencies while the SPL magnitude increases. At $f_b = 20$ Hz, the strongest response is concentrated in a relatively higher-frequency band around 700–980 Hz. At $f_b = 32$ Hz, the dominant band shifts to an intermediate range near 500–700 Hz, whereas at $f_b = 47$ Hz the strongest SPL is localized further in the lower-frequency range of approximately 400–550 Hz. The largely horizontal nature of these bands indicates a quasi-stationary acoustic response over time. This progressive shift toward lower frequencies, together with the increase in SPL, suggests enhanced bubble interaction and collective oscillation effects at higher bubbling rates.

CONCLUSIONS

The synchronized high-speed imaging and acoustic measurements were carried out for three bubbling rates, $f_b = 20$, 32, and 47 Hz. Acoustic measurements were performed in two distinct regimes. The first was in the near-nozzle region, at an axial distance of 10 cm from the nozzle, to capture the acoustic pressure radiated due to bubble dynamic events such as necking, detachment, impingement, and primary as well as secondary coalescence. The second measurement location was 20 cm downstream of the nozzle, where fragmentation and coupling effects associated with the presence of a long bubble

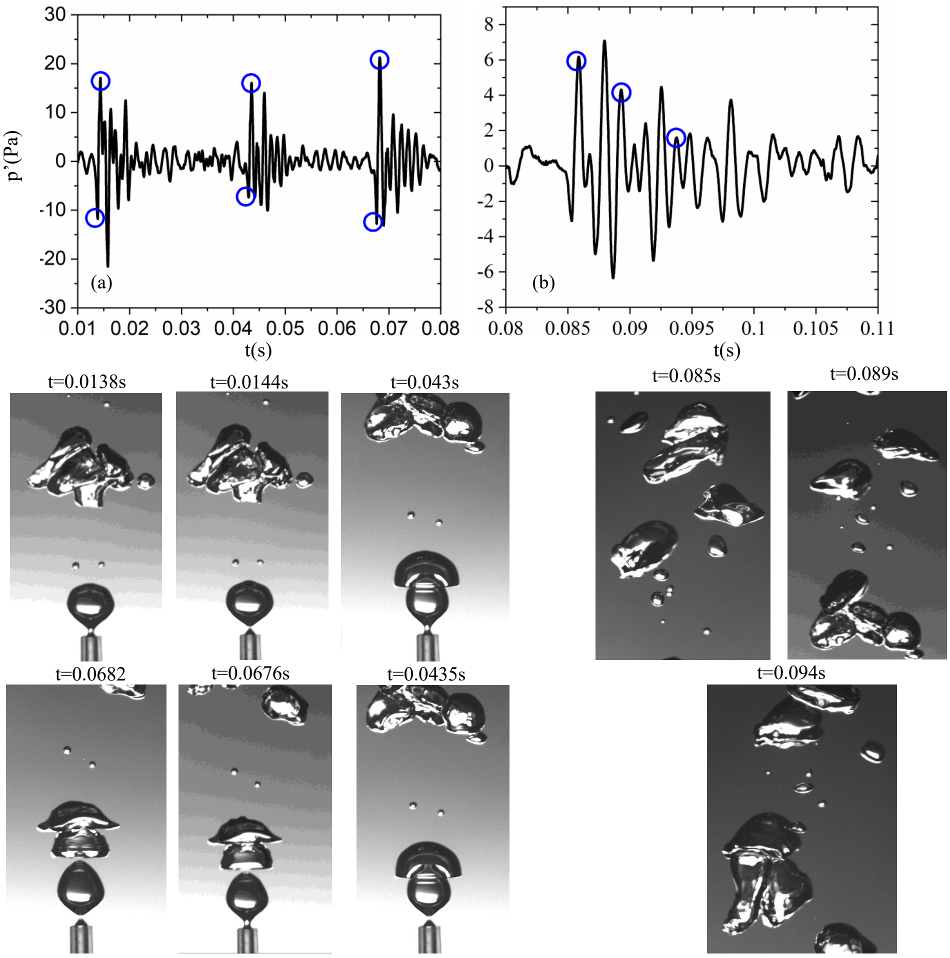

Figure 4. Acoustic response of the bubble chain at a bubbling rate of $f_b = 47$ Hz The circled time instants indicate the corresponding events identified in the synchronized shadowgraph images.

chain were predominantly observed. The key findings from the synchronization of bubble events with their corresponding acoustic response are summarized as follows:

1. A negative dip and rise in acoustic pressure is observed near the nozzle at all bubbling rates, f_b, which corresponds to the necking and volumetric pulsation and it increases with rise in f_b.
2. Among the observed events, volumetric pulsation during bubble pinch-off produces the strongest acoustic emission, whereas impingement and coalescence contribute more weakly due to their predominantly shape-oscillation character.
3. The bubbles present in the chain absorb energy from the newly detached bubble, and the subsequent oscillation of these bubbles modifies the measured acoustic response due to coupled oscillation effects from multiple oscillators in chain.
4. The energy spectra and SPL spectrogram indicate that a greater proportion of acoustic energy is concentrated near the nozzle than farther downstream, and this acoustic intensity increases with increasing f_b.
5. Complex interaction events, including primary coalescence, secondary coalescence, impingement, and detachment, contribute significantly to the acoustic energy and lead to broadening of the dominant narrowband frequency region.
6. Farther downstream, the coupled oscillations of multiple bubbles broaden the narrow frequency band owing to the phase lag among the bubbles in the chain. In contrast, the fragmented bubbles remain closely spaced and tend to oscillate collectively, thereby shifting the dominant response toward the lower-frequency region.

REFERENCES

Feuillade, C. 2001 Acoustically coupled gas bubbles in fluids: Time-domain phenomena. *The Journal of the Acoustical Society of America* **109** (6), 2606–2615.

Hsiao, P-Y, Devaud, Martin & Bacri, J-C 2001 Acoustic coupling between two air bubbles in water. *The European Physical Journal E* **4** (1), 5–10.

Leighton, Timothy 2012 *The acoustic bubble*. Academic press.

Longuet-Higgins, M. S. 1989 Monopole emission of sound by asymmetric bubble oscillations. part 1. normal modes. *Journal of Fluid Mechanics* **201**, 525–541.

Manasseh, Richard, Nikolovska, Aneta, Ooi, Andrew & Yoshida, Shizuo 2004 Anisotropy in the sound field generated by a bubble chain. *Journal of Sound and Vibration* **278** (4-5), 807–823.

Minnaert, Marcel 1933 Xvi. on musical air-bubbles and the sounds of running water. *The London, Edinburgh, and Dublin Philosophical Magazine and Journal of Science* **16** (104), 235–248.

Rayleigh, Lord 1917 Viii. on the pressure developed in a liquid during the collapse of a spherical cavity. *The London, Edin-*

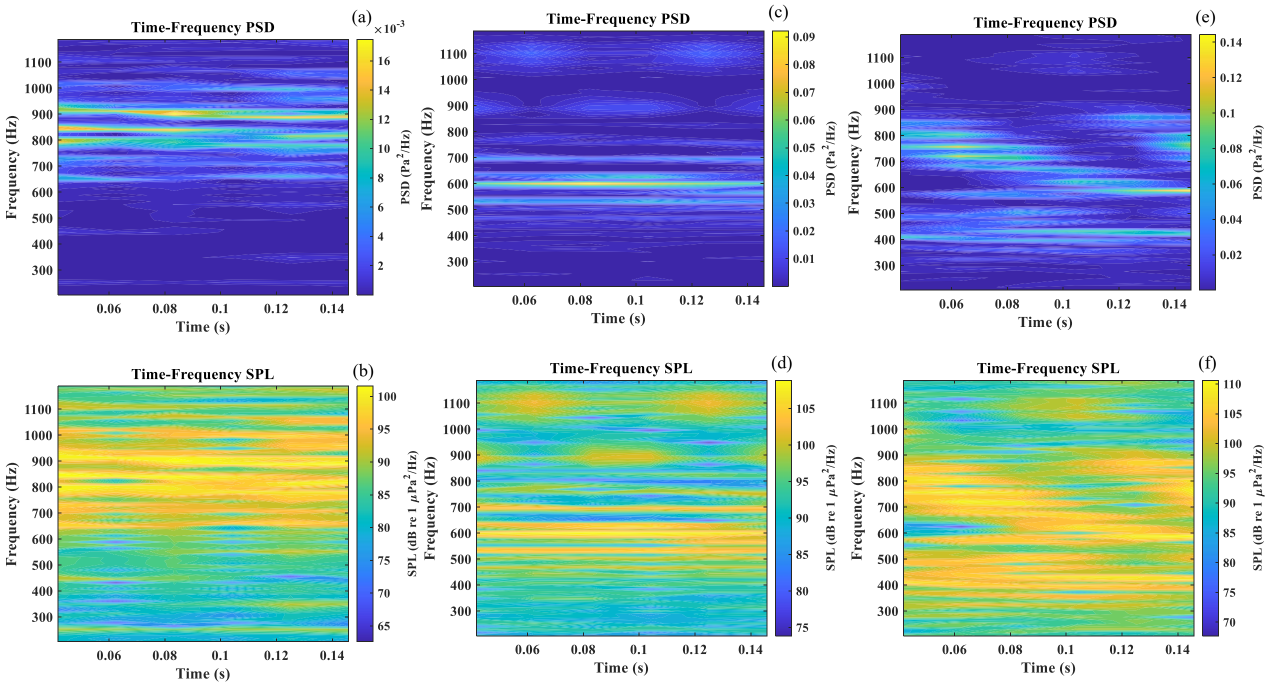

Figure 5. Spectral characteristics and sound pressure levels at different bubbling rates, f_b, in the near-nozzle regime. Panels (a), (c), and (e) show the PSD, while panels (b), (d), and (f) show the corresponding SPL for $f_b = 20$, 32, and 47 Hz, respectively.

.

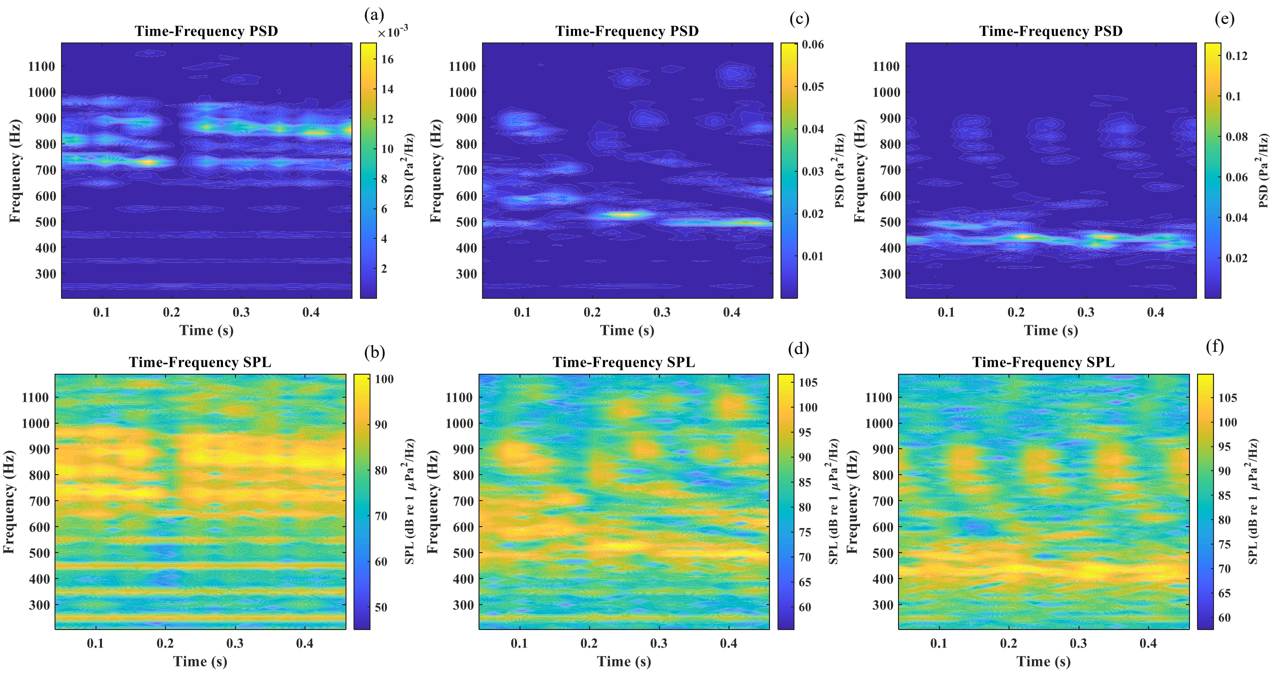

Figure 6. Spectral characteristics and sound pressure levels at different bubbling rates, f_b, measured in the downstream regime located 20 cm away from the nozzle. Panels (a), (c), and (e) show the PSD, while panels (b), (d), and (f) show the corresponding SPL for $f_b = 20$, 32, and 47 Hz, respectively.

burgh, and Dublin Philosophical Magazine and Journal of Science **34** (200), 94–98.

Strasberg, Murray 1956 Gas bubbles as sources of sound in liquids. *The Journal of the Acoustical Society of America* **28** (1), 20–26.

Tolstoy, I. 1986 Superresonant systems of scatterers. i. *The Journal of the Acoustical Society of America* **80** (1), 282–294.